

Of heading, posture and body rotations derived from data acquired by animal-borne accelerometers, magnetometers and gyrometers, kernel density estimation of the corresponding spherical distributions, and fine-scale movement reconstruction

Simon Benhamou
CEFE – CNRS Montpellier, France
Associated to Cogitamus Lab
simon.benhamou@cefe.cnrs.fr

Abstract. This paper provides the mathematical expressions, formulated in classical trigonometric terms, that are required (i) to compute an animal's body orientations and rotations in 3D space from data acquired at high-frequency by on-board accelerometers, magnetometers and gyrometers, (ii) to relate 3D rotations to changes in 3D orientation, (iii) to represent their spherical distributions through kernel density estimation (KDE), and (iv) to reconstruct fine-scale movements. The way the huge amount of data that is acquired by these on-board devices can be more easily managed is also considered.

1. Introduction

Thanks to a number of technological improvements, there has been an increase in the interest of deploying animal-borne loggers to investigate how animals move at various scales, and thus to attempt to elucidate the underlying behaviors (Williams et al. 2020). In particular, three types of high-frequency (>10 Hz) tri-axial bio-logger are commonly used nowadays to study movements performed at very small scale: accelerometers, magnetometers and gyrometers, which make it possible to assess 3D orientations and rotations.

My aim here is to provide a consistent and rational guide to the treatment of the data acquired by these loggers. A part of this information can be gathered in books on aeronautics or robotics, but is usually expressed in terms of complex mathematical formulae (e.g. involving quaternions). Same or other pieces of information, expressed in classical terms, more easily understandable by biologists/behavioral ecologists, of trigonometric functions were published in bio-logging oriented papers, but in a rather scattered way and they are not always reliable. In what follows, I will provide the mathematical expressions, formulated in classical trigonometric terms, that are required (i) to compute an animal's body orientations and rotations in 3D space from data acquired at high-frequency by on-board accelerometers, magnetometers and gyrometers, (ii) to relate 3D rotations to changes in 3D orientation, (iii) to represent their spherical distributions through kernel density estimation (KDE), and (iv) to reconstruct fine-scale movements. I will also consider how to manage the huge amount of data that are acquired by these on-board devices. I will focus mainly on loggers assumed to have been tightly set on the animal (usually on its back) in such a way that the device's

posture reflects the body posture. Much less information can be obtained when the logger is set on a collar, liable to roll around the neck. I will consider it only for reconstructing 2D fine-scale movements of a terrestrial animal.

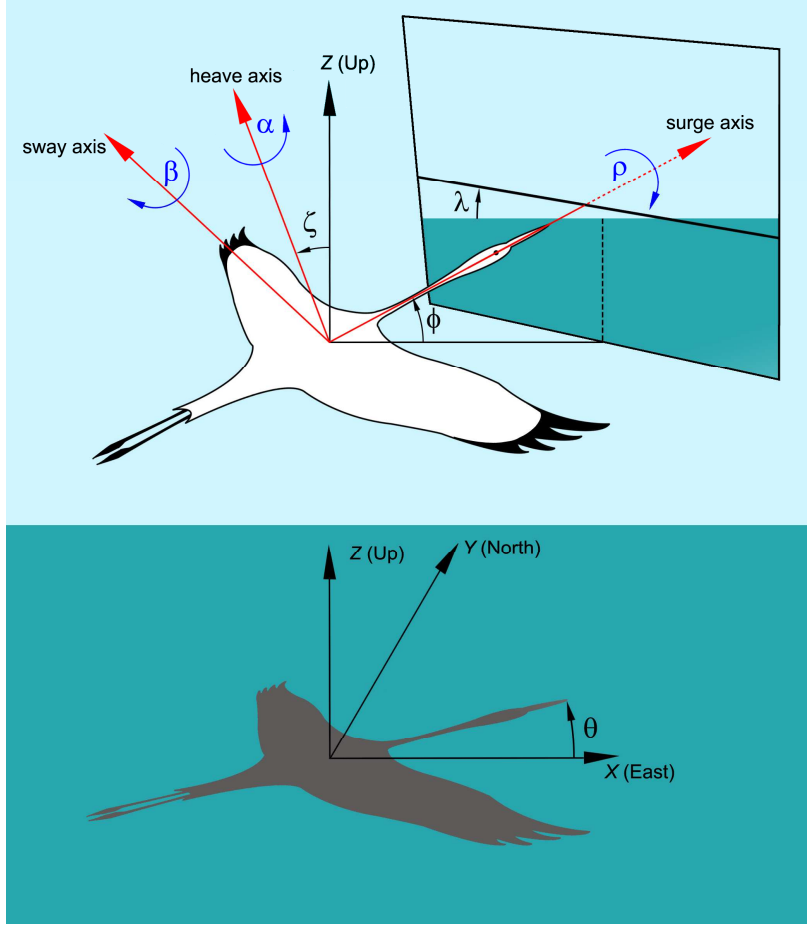


Fig. 1. Representation of various axes and angles. Let us consider a bird flying above a body of water. The XY plane, corresponding to the water surface, is horizontal, with the Earth-bound axes X pointing to East and Y pointing to North, while the Earth-bound axis Z points upwards (ENU convention). The animal-bound axes, referred to as the surge, sway and heave axes, correspond to the tail→head, right→left and belly→back axes, respectively. The 3D *orientation* is defined by the azimuth, θ , the elevation angle, ϕ , and the bank angle λ . The azimuth is the horizontal component of heading. It corresponds to the orientation of surge axis in the XY plane. The elevation angle corresponds to the orientation the surge axis, measured from the horizontal plane in the vertical plane at azimuth θ . It acts as both the vertical component of heading and the longitudinal component of posture. The bank angle is the transversal component of posture. It is measured from the horizontal

level in the animal's frontal plane (i.e. orthogonally to the surge axis) and corresponds to the orientation of the sway axis in this plane. The overall body inclination, ζ , combines the longitudinal (ϕ) and transversal (λ) components of posture. It corresponds to the deviation of the heave axis from the Z axis. Yaw, α , pitch, β , and roll, ρ , are *rotations* expressed in the animal-bound frame of reference: they are done around the three main body axes. The way these 3D rotations are related to the changes of heading and posture is addressed in §6.

Two frames of reference need to be considered. One is Earth-bound. It is defined by the three orthogonal axes X , Y and Z , which, throughout this paper, will conform the so-called East-North-Up (ENU) convention. The other is animal's body-bounded. It is defined by the surge (U), sway (V) and heave (W) axes, corresponding respectively to the tail→head (posterior-anterior), right→left (transversal), and belly→back (ventro-dorsal) axes (Fig. 1). They are orthogonal to, respectively, the frontal (sway x heave) plane, the sagittal (surge x heave) plane and the coronal (surge x sway) plane (in the few species moving in a stand-up posture, such as humans, the frontal and coronal planes are swapped because the surge axis then corresponds to the back→belly rather than tail→head axis). The direction of the surge axis (tail→head) was chosen to reflect the usual forward movement direction. The directions

of the sway (right→left) and heave axes (belly→back) were then set so to have the relative orientations of the three body axes, U , V and W , that match those of the X , Y and Z axes, respectively. The three body directions therefore follow the 'right-hand rule' with the index, middle finger and thumb representing the surge, sway and heave axes respectively.

Heading corresponds to the surge axis orientation expressed in the Earth-bound frame of reference. In 3D space, it is specified by two angular spherical coordinates, hereafter referred to as the azimuth, $\theta \in [-\pi, \pi]$, measured in the horizontal (XY) plane, and the elevation angle, $\phi \in [-\pi/2, \pi/2]$, measured vertically from the XY plane. Classically, the terms 'azimuth' and 'elevation angle' correspond to the compass bearing and angular elevation above the horizon line of an actual object. By extension, they are used here to specify the heading as the compass bearing and angular elevation of a virtual object towards which the animal would move. The posture corresponds to the body orientation with respect to gravity. It is usually specified in terms of longitudinal and transversal inclinations. The former corresponds to the elevation angle, $\phi \in [-\pi/2, \pi/2]$, which is therefore a component of both heading and posture. The latter, $\lambda \in [-\pi, \pi]$, referred to as the bank angle, corresponds to the orientation of the sway axis with respect to the horizontal level in the frontal plane (i.e. orthogonally to the surge axis; Fig. 1). It is sometimes mistaken for the vertical orientation of the sway axis measured from the horizontal (XY) plane, ϕ' (the way λ and ϕ' are related is highlighted in §2). Overall, the 3D orientation is therefore unequivocally specified by the three Euler/Tait-Bryan angles (θ , ϕ , λ). With the ENU convention, one gets $\theta = 0$ when the surge axis points eastwards and $\theta = \pi/2$ when it points northwards, and $\phi > 0$ and $\lambda > 0$ when the surge and sway axes, respectively, point above the horizon line. The azimuth, θ , elevation angle, ϕ , and bank angle, λ , which correspond to *orientations* expressed in the *Earth-bound* frame of reference, or the changes in these orientations, are often wrongly referred to as yaw, pitch and roll, which correspond to *rotations* expressed in the *body-bound* frame of reference (see §6).

In what follows, the key trigonometric relationships will be expressed using rotation matrices. They provide an easy way to determine the new Cartesian coordinates of a vector that was rotated by a given angle φ in a fixed frame of reference or, equivalently, that was kept fixed while the frame of reference was rotated by $-\varphi$. Depending on whether the rotation is done around the first (X or U), second (Y or V) or third (Z or W) axis, these matrices are:

$$\mathbf{R}_1(\varphi) = \begin{pmatrix} 1 & 0 & 0 \\ 0 & \cos(\varphi) & -\sin(\varphi) \\ 0 & \sin(\varphi) & \cos(\varphi) \end{pmatrix}, \mathbf{R}_2(\varphi) = \begin{pmatrix} \cos(\varphi) & 0 & -\sin(\varphi) \\ 0 & 1 & 0 \\ \sin(\varphi) & 0 & \cos(\varphi) \end{pmatrix}, \mathbf{R}_3(\varphi) = \begin{pmatrix} \cos(\varphi) & -\sin(\varphi) & 0 \\ \sin(\varphi) & \cos(\varphi) & 0 \\ 0 & 0 & 1 \end{pmatrix}$$

where φ is measured positively *counterclockwise* for \mathbf{R}_1 and \mathbf{R}_3 , but *clockwise* for \mathbf{R}_2 (in agreement with the ENU convention) when the rotation axis considered points towards the observer. The vector that stands for heading or posture is usually specified by two angular spherical coordinates, $\xi \in [-\pi, \pi]$ and $\psi \in [-\pi/2, \pi/2]$, which correspond to azimuth and elevation angle (θ , ϕ), or to bank and elevation angles (λ , ϕ). For simplicity, the equivalent

Cartesian form, $(\cos(\xi)\cos(\psi), \sin(\xi)\cos(\psi), \sin(\psi))$, will be written hereafter with the compact notation $[\xi \bullet \psi]$. Rotation matrices apply to its transpose $[\xi \bullet \psi]^T$ (i.e., with the three Cartesian coordinates written in a column rather than in a row).

2. Posture and activity estimation from 3D acceleration data

Accelerometers are sensitive to any type of linear acceleration, including gravity. An animal-borne high-frequency tri-axial accelerometer therefore makes it possible to determine both the body posture (i.e. the orientation with respect to gravity) and the activity level, once the 'static' (gravity-induced) and 'dynamic' (movement-induced) components have been disentangled.

Call $\mathbf{a} = (a_U, a_V, a_W)$ the acceleration vector recorded at any given time t , where a_U , a_V , and a_W corresponds to the values obtained for the surge, sway and heave axes of the accelerometer, respectively. When this device is at rest, one gets $\|\mathbf{a}\| = g$ (9.81 m/s²), while the value obtained for each axis ranges between $-g$ and g , depending on its orientation ($-g$ when the axis considered is kept vertically upwards, g when it is kept vertically downwards, 0 when it is kept horizontal). When the device is borne by a moving animal, the data obtained for each axis corresponds to the combination of a static and a dynamic components. Assuming that dynamic acceleration involves mainly fluctuations that tend to quickly counter-balance each other, the static acceleration at time t can be accounted for by the mean vector $\bar{\mathbf{a}} = (\bar{a}_U, \bar{a}_V, \bar{a}_W)$, where \bar{a}_U , \bar{a}_V , \bar{a}_W are the mean values obtained for each axis separately, by averaging the values recorded between times $t - \Delta t/2$ and $t + \Delta t/2$. The temporal window Δt must be long enough to smooth acceleration fluctuations but short enough to keep the best possible resolution. A width ranging between 1 and 3 s (depending on the species; Shepard et al. 2008a) is usually appropriate. The norm of the static acceleration, $\|\bar{\mathbf{a}}\| = (\bar{a}_U^2 + \bar{a}_V^2 + \bar{a}_W^2)^{0.5}$, should usually remain close to g (otherwise the temporal window Δt has to be enlarged). As it cannot be set at the body mass center, an accelerometer is also subjected to linear accelerations due to body rotations, which may result in underestimating the norm of the static acceleration $\|\bar{\mathbf{a}}\|$ (in contrast, the mean norm $\|\bar{\mathbf{a}}\|$ should remain close to g). However, the device is usually set sufficiently close to the body mass center to consider that values of a_U , a_V and a_W obtained reflect almost purely linear movements.

The device has to be tightly set on the animal's back in such a way that its surge axis lies in the body's sagittal plane. However, as the animal's back may not be flat, the device may have been set in a somewhat tilted way, longitudinally (around the sway axis) by ϕ^* , and/or transversally (around the surge axis) by λ^* . Thus, the body posture may somewhat differ from the device's posture. The static acceleration vector of the freely moving animal, $\mathbf{A} = (A_U, A_V, A_W)$ can be derived from the static acceleration vector of the device, $\bar{\mathbf{a}}$, based on the relationship $\mathbf{A}^T = \mathbf{R}_2(\phi^*)\mathbf{R}_1(\lambda^*)\bar{\mathbf{a}}^T$, i.e.

$$A_U = \cos(\phi^*)\bar{a}_U - \sin(\phi^*)(\sin(\lambda^*)\bar{a}_V + \cos(\lambda^*)\bar{a}_W) \quad (1a)$$

$$A_V = \cos(\lambda^*)\bar{a}_V - \sin(\lambda^*)\bar{a}_W \quad (1b)$$

$$A_W = \sin(\phi^*)\bar{a}_U + \cos(\phi^*)(\sin(\lambda^*)\bar{a}_V + \cos(\lambda^*)\bar{a}_W) \quad (1c)$$

with $\phi^* = \sin^{-1}(-a_U^* / \|\mathbf{a}^*\|)$ and $\lambda^* = \text{atan}_2(-a_V^*, -a_W^*)^1$, where $\mathbf{a}^* = (a_U^*, a_V^*, a_W^*)$ is the acceleration vector recorded by the device set on the animal that was kept level before release. Note that the norm is not affected by the tilt: $\|\mathbf{A}\| = \|\mathbf{a}\|$. The body posture can then be specified by the vertical orientations, measured from the horizontal plane, of its surge axis, $\phi = \sin^{-1}(-A_U / \|\mathbf{A}\|)$, sway axis, $\phi' = \sin^{-1}(-A_V / \|\mathbf{A}\|)$, and heave axis, $\phi'' = \sin^{-1}(-A_W / \|\mathbf{A}\|)$. As these three axes are orthogonal to each other, the body posture can be specified unequivocally by only two angles, which correspond to the two angular spherical coordinates of a unit vector whose Cartesian coordinates are $\sin(\phi)$, $\sin(\phi')$ and $\sin(\phi'')$. The body posture can thus be expressed in terms of overall inclination,

$$\zeta = \pi/2 - \phi'' = \cos^{-1}(-A_W / \|\mathbf{A}\|), \quad (2a)$$

which measures the angular deviation between the heave axis and the Z (upward vertical) axis, and postural orientation,

$$\chi = \text{atan}_2(\sin(\phi'), \sin(\phi)) = \text{atan}_2(-A_V, -A_U), \quad (2b)$$

which corresponds to the body-related orientation (forwards-backwards and/or rightwards-leftwards) in which the deviation from the Z axis occurs. This handy representation, based on $[\chi \bullet \phi''] = (\sin(\phi), \sin(\phi'), \sin(\phi''))$, is comparable to a spherical bull's eye spirit level whose equatorial plane stands for the device's coronal plane and bubble stands for the Z axis direction. It is however often more convenient, for subsequent computations, to specify the posture in terms of elevation angle,

$$\phi = \sin^{-1}(-A_U / \|\mathbf{A}\|) = \tan^{-1}(-A_U / (A_V^2 + A_W^2)^{0.5}), \quad (3a)$$

and bank angle, which corresponds to the orientation of the sway axis measured in the frontal plane from the horizontal level,

$$\lambda = \text{atan}_2(\sin(\phi'), \sin(\phi'')) = \text{atan}_2(-A_V, -A_W), \quad (3b)$$

based on $[\lambda \bullet \phi] = (\sin(\phi''), \sin(\phi'), \sin(\phi))$. The overall body inclination can be easily derived from the elevation and bank angles through the relationship $\cos(\zeta) = \cos(\phi) \cos(\lambda)$.

An accelerometer being an inertial measurement device, any movement-induced acceleration is recorded as the result of an apparent force acting in the reverse direction: backward for a forward acceleration, forward for a backward acceleration (i.e. deceleration), centrifugal for the centripetal acceleration involved in turning. The body posture estimates obtained using Eqs (2) and (3) are expressed with respect to a reference plane that is orthogonal to this apparent force. As movement-induced accelerations tend to counter-balance each other over Δt , only gravity should matter ($\|\mathbf{A}\| \approx g$) and the reference plane remains (roughly) horizontal. However, this plane will be somewhat tilted when an animal undertakes a strong long-lasting forward, backward or centripetal acceleration (e.g., a bird taking off, landing, or gliding along a circle arc, respectively; e.g. Williams et al. 2015). Determining the body posture in this context is quite complex. Just to get a flavor, consider an animal that

¹ $\text{atan}_2(y, x) = \tan^{-1}(y/x) \pm b\pi$ with $b=0$ for $x>0$ and $b=1$ for $x<0$

accelerates in the horizontal plane (i.e., orthogonally to gravity), either tangentially or centripetally. In this simple example, one gets $\|\mathbf{A}\| \approx (g^2 + h^2)^{0.5}$, with $h = \Delta v / \Delta t$ for a tangential acceleration, or $h = v^2 / r$ for a centripetal acceleration, where v is the linear speed and r is the radius of curvature. The reference plane is tilted by $\tan^{-1}(h/g)$ with respect to the horizontal plane, either longitudinally for a tangential acceleration or transversally for a centripetal acceleration. The bank angle has then to be corrected: $\phi = \sin^{-1}(-A_U / \|\mathbf{A}\|) - \tan^{-1}(\Delta v / (g \Delta t))$ in the former case, $\lambda = \text{atan}_2(-A_V, -A_W) \pm \tan^{-1}(v^2 / (gr))$ ($-$ for a left turn, $+$ for a right turn) in the latter case. Thus, for a turn at constant speed in the horizontal plane, a car with stiff suspensions will show no banking ($\lambda = 0$) while it is submitted to a strong transversal acceleration ($|A_V| = v^2 / r$), whereas a bicycle has to adopt the bank angle $\lambda = \pm \tan^{-1}(v^2 / (gr))$ to turn as expected while it is submitted to no noticeable transversal acceleration ($A_V \approx 0$). Analyses of the flights of a griffon vulture and an osprey (O. Duriez, unpublished data) showed that, unsurprisingly, the 'bicycle way' applies to soaring birds that loop in a thermal to gain altitude.

The data acquired with the accelerometer can also be used to assess activity level as the mean of the norm, $\|\mathbf{d}\| = (d_U^2 + d_V^2 + d_W^2)^{0.5}$, of the vector difference, $\mathbf{d} = (d_U, d_V, d_W) = \mathbf{a} - \bar{\mathbf{a}}$. The value of $\|\mathbf{d}\|$ will be referred hereafter to as the 'Dynamic Body Acceleration' (DBA). The DBA value computed in this way does not depend on the posture. It can therefore be considered a reliable is reliable measure of activity, including when the device is set on a collar (i.e. when the device's posture may be markedly different from the body posture). It was initially called (somewhat misleadingly, as it is a scalar) 'vectorial DBA' (veDBA) by Qasem et al. (2012), to distinguish it from the previous, mathematically inconsistent, way to combine the three \mathbf{d} components, $|d_U| + |d_V| + |d_W|$, called 'overall DBA' (ODBA; Wilson et al. 2006), which results in unreliable (posture-dependent) activity values. On average, DBA is proportional to oxygen consumption and therefore can act as a suitable proxy for energetic expenses (Gleiss et al. 2011, Qasem et al. 2012; Wilson et al. 2020). It can also provide a proxy for the linear speed (see §8).

Static and dynamic accelerations, \mathbf{d} and $\bar{\mathbf{a}}$, have initially to be computed at the same high frequency f as the frequency with which raw data, \mathbf{a} , is acquired by using a *sliding* Δt -width window, with $\bar{\mathbf{a}}$ being attributed to the center of the window, which encompasses $k = \text{round}(f \Delta t)$ values. Depending on whether k is odd or even, $\bar{\mathbf{a}}$ has to be computed by averaging the $(k-1)/2$ or $(k-2)/2$ preceding values, the central value, and the $(k-1)/2$ or $(k-2)/2$ following values. Nevertheless, the amount of data to process in subsequently analyses can be dramatically reduced (divided by k) by keeping, for each time step Δt , a single $\bar{\mathbf{a}}$ through subsampling (i.e. as if $\bar{\mathbf{a}}$ was computed using a *jumping* rather than *sliding* window), and a single DBA value through averaging (see §9).

3. Heading estimation from 3D accelero-magnetic data

Heading in 3D space is defined by both azimuth, θ , and elevation angle, ϕ . While the latter only requires a high-frequency tri-axial accelerometer to be estimated (Eq. 3a), the former requires a tri-axial high frequency accelero-magnetometer. Indeed, a tri-axial magnetometer, which records the geomagnetic field in 3D space, makes it possible to compute the azimuth with respect to the magnetic North only if its posture is known. For this purpose, it must be tightly associated with an accelerometer (on the same chip, sharing the same axes, and being synchronized with a common clock, but not necessarily working at the same frequency).

A magnetometer must be properly calibrated. Indeed, a shift of the range of the values obtained (offset), specific to each axis, is expected because the device itself generates a magnetic field (hard iron effect). The sensitivity on each axis may also be affected by the local environment (soft iron effect). The gains and offsets have therefore to be adjusted to obtain calibrated values expressed in the same 0-centered range for the three axes. The range width by itself does not matter. If the identities of the three axes (surge, sway and heave) and their directions are known, a simple way to calibrate the magnetometer consists in rotating it at random (in 3D) for a while. Then, for each axis separately, call r_{\min} and r_{\max} the minimum and maximum values of the raw magnetic values acquired during this random rotation. Any raw value r can then be translated into a calibrated one as $m = s(2r - r_{\min} - r_{\max}) / (r_{\max} - r_{\min})$, with $s = 1$ or $s = -1$ depending on whether the maximum value of r is obtained when the axis considered points northwards or southward, respectively. Another, more rigorous, procedure is as follows. Call (N_U, N_V, N_W) , (E_U, E_V, E_W) , (S_U, S_V, S_W) , and (W_U, W_V, W_W) , the raw magnetic values measured for the surge (U), sway (V) and heave (W) axes when the surge axis, kept horizontal, points successively towards magnetic North, East, South and West, respectively. These values must be acquired twice, through two horizontal rotations of the surge axis: (i) with the device that rests on its bottom ($a_U = a_V = 0$, $a_W = -g$), and (ii) with the device that rests on its left ($a_U = a_W = 0$, $a_V = \|\mathbf{a}\|$) or right ($a_U = a_W = 0$, $a_V = -\|\mathbf{a}\|$) flank. The 'bottom' rotation should let the W -indexed values unchanged and result in $E_U \approx W_U \approx (N_U + S_U)/2$ and $N_V \approx S_V \approx (E_V + W_V)/2$, whereas the 'flank' rotation should let the V -indexed values unchanged and result in $N_W \approx S_W \approx (E_W + W_W)/2$ and in U -indexed values alike those obtained with the 'bottom' rotation (otherwise, swap the labels of the axes). The raw magnetic values, r_U , r_V and r_W can then be translated into the calibrated ones m_U , m_V and m_W as:

$$m_U = (2r_U - N_U - S_U) / (N_U - S_U) \quad \text{based on the 'bottom' rotation} \quad (4a)$$

$$m_V = (2r_V - E_V - W_V) / (E_V - W_V) \quad \text{based on the 'bottom' rotation} \quad (4b)$$

$$m_W = s(2r_W - E_W - W_W) / (E_W - W_W), \quad \text{based on the 'flank' rotation} \quad (4c)$$

with $s = 1$ or $s = -1$ depending on whether the 'flank' rotation was made on the right or left side, respectively. Thus, for any axis that is rotated in the horizontal plane, the calibrated values vary from -1 (when the axis considered points southwards) to 1 (when it points northwards). The actual magnetic values can be obtained by multiplying each calibrated value

by $B\cos(\varphi)$, where B is the local geomagnetic field intensity and φ is the geomagnetic dip angle (inclination). However, these two parameters can be fully ignored, because the azimuth estimate rests on the ratio of two calibrated values (see below).

Call $\bar{\mathbf{m}} = (\bar{m}_U, \bar{m}_V, \bar{m}_W)$ the mean calibrated magnetic vector obtained by averaging the magnetic values acquired, for each axis, separately over the short time interval Δt (in practice, it is faster and mathematically equivalent to average the raw magnetic values first and then to correct the mean values). The measures made by the device are expressed in its own frame of reference, which may differ from the animal's one. To avoid the challenging procedure (see Johnson & Tyack 2003) that would be required otherwise, the device must be set on the animal in such a way that its surge axis lies in the body sagittal plane. However, because the animal's back may not be flat, the device may have been set tilted transversally by λ^* (but this does not affect heading) and longitudinally by ϕ^* . If so, the device's azimuth will differ from the body azimuth when the animal moves banked. The body-related mean magnetic vector $\mathbf{M} = (M_U, M_V, M_W)$ can be derived from the device-related one $\bar{\mathbf{m}}$ as $\mathbf{M}^T = \mathbf{R}_2(\phi^*)\mathbf{R}_1(\lambda^*)\bar{\mathbf{m}}^T$, i.e.

$$M_U = \cos(\phi^*)\bar{m}_U - \sin(\phi^*)(\sin(\lambda^*)\bar{m}_V + \cos(\lambda^*)\bar{m}_W) \quad (5a)$$

$$M_V = \cos(\lambda^*)\bar{m}_V - \sin(\lambda^*)\bar{m}_W \quad (5b)$$

$$M_W = \sin(\phi^*)\bar{m}_U + \cos(\phi^*)(\sin(\lambda^*)\bar{m}_V + \cos(\lambda^*)\bar{m}_W) \quad (5c)$$

The body azimuth can then be assessed by combining the body-related static acceleration vector \mathbf{A} and mean magnetic vector \mathbf{M} . Call $\underline{\mathbf{M}} = (\underline{M}_U, \underline{M}_V, \underline{M}_W)$ the mean magnetic vector that would have been obtained if the body was leveled while keeping its azimuth θ unchanged: $\underline{\mathbf{M}}^T = \mathbf{R}_2(\phi)\mathbf{R}_1(\lambda)\mathbf{M}^T$, where ϕ and λ are the body elevation and bank angles (Eqs 3). The magnetic North azimuth expressed with respect to the body surge axis is equal to $\text{atan}_2(\underline{M}_V, \underline{M}_U)$. The body azimuth, measured positively counterclockwise with respect to magnetic East, $\theta = \pi/2 - \text{atan}_2(\underline{M}_V, \underline{M}_U) = \text{atan}_2(\underline{M}_U, \underline{M}_V)$, can therefore be computed as

$$\theta = \text{atan}_2((A_V^2 + A_W^2)M_U - A_U(A_V M_V + A_W M_W), (A_V M_W - A_W M_V) \|\mathbf{A}\|) \quad (6)$$

If necessary, the 'true' azimuth value (i.e. based on geographical East) can be obtained by subtracting the geomagnetic declination. However, for fine-scale movement reconstruction, this magnetic parameter can also be ignored (see §8). In the particular case of an animal that heads up or down ($\phi \approx \pm \pi/2$, $A_V \approx A_W \approx 0$), the azimuth (and bank angle) becomes irrelevant: its estimates vary randomly due to noise in \mathbf{a} and \mathbf{m} measures. Complementary information can then be provided by the orientation of the sway axis, $\theta' = \text{atan}_2(M_V \|\mathbf{A}\|, -A_U M_W)$.

4. Rotation estimations from 3D gyroscopic data

A high-frequency tri-axial gyrometer measures the angular velocity components in the coronal, sagittal and frontal planes. They are referred to as yaw, pitch and roll speeds, $\dot{\alpha}$, $\dot{\beta}$ and $\dot{\rho}$, respectively. To be consistent with the ENU convention, $\dot{\alpha}$ and $\dot{\rho}$ are positive but $\dot{\beta}$ is negative for a rotation that appears anticlockwise when the corresponding rotation axis points towards the observer (beware that the convention used in the firmware of the device

may be different). Gyrometers are easy to use. However, it must be kept in mind that the angular speed measures obtained concern the device, and may therefore differ from the angular speeds of the animal if the device and the body are not perfectly aligned. As previously, let us assume that the device, set on an animal's back, was set in such a way that its surge axis lies in the animal's sagittal plane but may have been tilted longitudinally by ϕ^* and/or transversally by λ^* . The body-related angular velocity $(\dot{\rho}, -\dot{\beta}, \dot{\alpha})$ can then be derived from the recorded one $(\dot{\rho}^d, -\dot{\beta}^d, \dot{\alpha}^d)$ as $(\dot{\rho}, -\dot{\beta}, \dot{\alpha})^T = \mathbf{R}_2(\phi^*)\mathbf{R}_1(\lambda^*)(\dot{\rho}^d, -\dot{\beta}^d, \dot{\alpha}^d)^T$, i.e.

$$\dot{\alpha} = \sin(\phi^*)\dot{\rho}^d + \cos(\phi^*)(\cos(\lambda^*)\dot{\alpha}^d - \sin(\lambda^*)\dot{\beta}^d) \quad (7a)$$

$$\dot{\beta} = \cos(\lambda^*)\dot{\beta}^d + \sin(\lambda^*)\dot{\alpha}^d \quad (7b)$$

$$\dot{\rho} = \cos(\phi^*)\dot{\rho}^d - \sin(\phi^*)(\cos(\lambda^*)\dot{\alpha}^d - \sin(\lambda^*)\dot{\beta}^d) \quad (7c)$$

The body-related rotations yaw, pitch and roll for a given time step $\Delta t = t_i - t_{i-1}$ can be computed simply as $\alpha_i = \sum_j \dot{\alpha}_{i,j} / f$, $\beta_i = \sum_j \dot{\beta}_{i,j} / f$ and $\rho_i = \sum_j \dot{\rho}_{i,j} / f$, for $j = 1 \dots k$, based on the $k = \text{round}(f\Delta t)$ angular speeds, $\dot{\alpha}_{i,j}$, $\dot{\beta}_{i,j}$ and $\dot{\rho}_{i,j}$ measured with the frequency f .

A high-frequency tri-axial gyrometer is the most reliable device for measuring yaw, pitch and roll. Without it, these three body rotations can be assessed indirectly from data acquired by a high-frequency tri-axial accelero-magnetometer (see §6). Reciprocally, changes of azimuth $\Delta\theta$ for a given time step Δt can be estimated using a high-frequency tri-axial accelero-gyrometer (Eq. 15). However, estimating the current azimuth as the sum of changes of azimuth and initial azimuth ($\theta_i = \sum_{j=1}^i \Delta\theta_j + \theta_0$) quickly accumulate random errors. Hence, accelero-gyrometers can be used in place of accelero-magnetometers to assess azimuth only at very short term. An accelero-magneto-gyrometer can be useful to cross-check heading estimates, but involves a non-negligible battery drain. It may help infer high-speed movements with great accuracy (Wilson et al. 2013), in particular because the tilting of the reference plane when the animal undertook strong long-lasting accelerations prevents suitable estimation of the posture based only on acceleration data (see §2).

5. Changes of heading and posture

A given heading can be represented as a point at the surface of a unit sphere centered on the animal's current location and whose reference axes (X, Y, Z) match the geographical ones (East, North, Up; Fig. 2). The change of heading is done in the plane defined by the two unit vectors, $[\theta_{i-1} \bullet \phi_{i-1}]$ and $[\theta_i \bullet \phi_i]$, standing for headings at two successive time steps. It can be characterized by the size, $\omega_i \in [0, \pi]$ and initial inclination, $\delta_i^i \in [-\pi, \pi]$, measured positively counterclockwise from the horizontal level in the animal's current frontal plane, i.e. tangentially to the unit sphere at the current heading, of the orthodromic arc that links these two points. It corresponds both to the shortest possible surface route (geodesic) and to the minor arc of the 'great circle', i.e. the largest circle that can be drawn on a sphere, passing

through the two points considered. Based on the relationship $[\theta_i \bullet \phi_i]^T = \mathbf{R}_3(\theta_{i-1})\mathbf{R}_2(\phi_{i-1})\mathbf{R}_1(\delta_i^i)$ $[\omega_i \bullet 0]^T$, the new heading can be computed as:

$$\theta_i = \theta_{i-1} + \text{atan2}(\cos(\delta_i^i), \cos(\phi_{i-1})/\tan(\omega_i) - \sin(\delta_i^i) \sin(\phi_{i-1})) \quad (8a)$$

$$\phi_i = \sin^{-1}(\sin(\omega_i) \sin(\delta_i^i) \cos(\phi_{i-1}) + \cos(\omega_i) \sin(\phi_{i-1})). \quad (8b)$$

Reciprocally, the size, ω_i , and the initial and final inclinations, δ_i^i and δ_i^f , of the change of heading from $(\theta_{i-1}, \phi_{i-1})$ to (θ_i, ϕ_i) , modeled as an orthodromic arc, can be computed as:

$$\omega_i = \cos^{-1}(\sin(\phi_i) \sin(\phi_{i-1}) + \cos(\phi_i) \cos(\phi_{i-1}) \cos(\theta_i - \theta_{i-1})) \quad (9a)$$

$$\delta_i^i = \text{atan2}(\sin(\phi_i) - \cos(\omega_i) \sin(\phi_{i-1}), \cos(\phi_i) \cos(\phi_{i-1}) \sin(\theta_i - \theta_{i-1})) \quad (9b)$$

$$\delta_i^f = \text{atan2}(\cos(\omega_i) \sin(\phi_i) - \sin(\phi_{i-1}), \cos(\phi_i) \cos(\phi_{i-1}) \sin(\theta_i - \theta_{i-1})) \quad (9c)$$

$$= \text{atan2}(\cos(\omega_i) \sin(\delta_i^i) - \sin(\omega_i) \tan(\phi_{i-1}), \cos(\delta_i^i))$$

Eqs (8) and (9) can also be partly derived from the spherical law of cosines. Eq. (9a) can also be easily found by remembering that the dot product of two unit vectors is simply equal to the cosine of angular discrepancy between them in the plane defined by these two vectors: $\cos(\omega_i) = [\theta_{i-1} \bullet \phi_{i-1}] \cdot [\theta_i \bullet \phi_i]$.

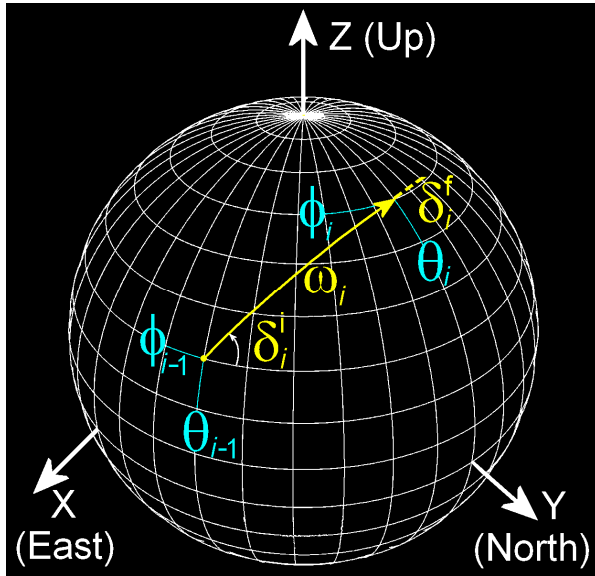


Fig. 2. Change from heading $[\theta_{i-1} \bullet \phi_{i-1}]$ to heading $[\theta_i \bullet \phi_i]$. Modeled as the orthodromic arc linking these two headings, this reorientation can be suitably represented on a unit sphere in a mixed body-bound/Earth-bound frame of reference: the sphere is centered on the animal's location $\mathbf{x}_{i-1} = (x_{i-1}, y_{i-1}, z_{i-1})$, but its reference directions are provided by the X axis pointing eastwards, the Y axis pointing northwards and the Z axis pointing upwards (ENU convention). Azimuths, θ_{i-1} and θ_i , are equivalent to longitudes while elevation angles, ϕ_{i-1} and ϕ_i , are equivalent to latitudes. The magnitude of the change of heading, i.e. the arc size ω_i , is an 'internal' angle whose vertex corresponds to the center of the unit sphere, while the initial and final arc inclinations, δ_i^i and δ_i^f , are 'surface' angles measured in the animal's current frontal plane, i.e. the plane orthogonal to the unit sphere at their respective vertices. In this example of a counterclockwise reorientation, the values of the

different angles are $\theta_{i-1} = \phi_{i-1} = \pi/6$, $\theta_i = \pi/2$, $\phi_i = \pi/3$, $\omega_i \approx \pi/3.637$, $\delta_i^i \approx \pi/3.256$ and $\delta_i^f \approx \pi/19.023$ (replace π by 180 to obtain values in degrees). The product $p = \cos(\phi_{i-1})\cos(\delta_i^i) = \cos(\phi_i)\cos(\delta_i^f)$ characterizes the inclination of the reorientation plane, $\phi_{\max} = \cos^{-1}(|p|) \approx \pi/2.978$, which also corresponds to the elevation angle of the highest point of the great circle to which the orthodromic arc belongs (reached at azimuth $\theta_{i-1} + \text{sgn}(\tan(\delta_i^i)) \cos^{-1}(\tan(\phi_{i-1})/\tan(\phi_{\max})) = \theta_i + \text{sgn}(\tan(\delta_i^f)) \cos^{-1}(\tan(\phi_i)/\tan(\phi_{\max})) \approx \pi/1.784$). For a counter-clockwise reorientation, $|\delta_i^i|$ and $|\delta_i^f|$ cannot be larger than ϕ_{\max} , while they cannot be smaller than $\pi - \phi_{\max}$ for a clockwise reorientation.

Similarly, the cosine of the size, ϖ_i , of the change of posture can be computed as

$$\cos(\varpi_i) = [\lambda_{i-1} \bullet \phi_{i-1}] \cdot [\lambda_i \bullet \phi_i] = [\chi_{i-1} \bullet \phi_{i-1}] \cdot [\chi_i \bullet \phi_i] = \mathbf{A}_{i-1} \mathbf{A}_i / (||\mathbf{A}_{i-1}|| ||\mathbf{A}_i||) \quad (10)$$

The heading/posture is expected to vary progressively for the time step $\Delta t = t_i - t_{i-1}$, from $(\theta_{i-1}, \phi_{i-1}, \lambda_{i-1})$ to $(\theta_i, \phi_i, \lambda_i)$. The change of heading for this short time interval can be assumed to be done at constant angular speed, $\omega_i/\Delta t$. The in-between azimuth, $\tilde{\theta}_i(q)$, elevation angle, $\tilde{\phi}_i(q)$, and reorientation inclination, $\tilde{\delta}_i(q)$, at time $t_{i-1} + q\Delta t$ with $q \in [0, 1]$ can then be

interpolated based on the relationship $[\tilde{\theta}_i(q) \cdot \tilde{\phi}_i(q)]^T = \mathbf{R}_3(\theta_{i-1})\mathbf{R}_2(\phi_{i-1})\mathbf{R}_1(\delta_i^i)[q\omega_i \cdot \mathbf{0}]^T$. The in-between azimuth and elevation angle are obtained simply by replacing ω_i with $q\omega_i$ in Eqs (8):

$$\tilde{\theta}_i(q) = \theta_{i-1} + \text{atan2}(\cos(\delta_i^i), \cos(\phi_{i-1})/\tan(q\omega_i) - \sin(\delta_i^i) \sin(\phi_{i-1})) \quad (11a)$$

$$\tilde{\phi}_i(q) = \sin^{-1}(\sin(q\omega_i) \sin(\delta_i^i) \cos(\phi_{i-1}) + \cos(q\omega_i) \sin(\phi_{i-1})) \quad (11b)$$

while the in-between reorientation inclination can be derived from Eq. (9c) as:

$$\begin{aligned} \tilde{\delta}_i(q) &= \text{atan2}(\cos(q\omega_i) \sin(\delta_i^i) - \sin(q\omega_i) \tan(\phi_{i-1}), \cos(\delta_i^i)). \\ &= \text{atan2}(\cos(q\omega_i)\sin(\phi_i) - \cos((1-q)\omega_i)\sin(\phi_{i-1}), \cos(\phi_{i-1})\cos(\phi_i)\sin(\theta_i - \theta_{i-1})) \end{aligned} \quad (11c)$$

They vary from $\tilde{\theta}_i(0) = \theta_{i-1}$, $\tilde{\phi}_i(0) = \phi_{i-1}$ and $\tilde{\delta}_i(0) = \delta_i^i$ at time t_{i-1} to $\tilde{\theta}_i(1) = \theta_i$, $\tilde{\phi}_i(1) = \phi_i$ and $\tilde{\delta}_i(1) = \delta_i^f$ at time t_i , while the product $\cos(\tilde{\phi}_i(q))\cos(\tilde{\delta}_i(q))$, which characterizes the inclination of the reorientation plane, remains constant. It is worth noting that the change of arc inclination from δ_i^i to δ_i^f corresponds to an intrinsic rotation of the frontal plane by $\delta_i^f - \delta_i^i$. This compels the bank angle $\tilde{\lambda}_i(q)$, which varies from $\tilde{\lambda}_i(0) = \lambda_{i-1}$ at time t_{i-1} to $\tilde{\lambda}_i(1) = \lambda_i$ at time t_i , to change passively (i.e. without involving any roll) by the same amount. If some roll occurs concomitantly, it simply adds to the passive change. Accordingly, the arc inclination expressed with respect to the coronal plane, $\tilde{\eta}_i(q) = \tilde{\delta}_i(q) - \tilde{\lambda}_i(q)$, which ranges from $\tilde{\eta}_i(0) = \eta_i^i = \delta_i^i - \lambda_{i-1}$ to $\tilde{\eta}_i(1) = \eta_i^f = \delta_i^f - \lambda_i$, remains constant ($\eta_i^f = \eta_i^i$) during any change of heading without rolling. Assuming that roll, $\rho_i = \eta_i^i - \eta_i^f$, is done at constant speed, $\rho_i/\Delta t$, between times t_{i-1} and t_i , the in-between bank angle can be interpolated as

$$\tilde{\lambda}_i(q) = \lambda_{i-1} + \tilde{\delta}_i(q) - \delta_i^i + q(\eta_i^i - \eta_i^f) = \tilde{\delta}_i(q) - q\eta_i^f - (1-q)\eta_i^i \quad (11d)$$

This pseudo-continuous approach warrants a smooth transition of heading/posture at discrete times t_i : $\tilde{\theta}_i(0) = \tilde{\theta}_{i-1}(1)$, $\tilde{\phi}_i(0) = \tilde{\phi}_{i-1}(1)$ and $\tilde{\lambda}_i(0) = \tilde{\lambda}_{i-1}(1)$. The time step, $\Delta t = t_i - t_{i-1}$, should be large enough to smooth the recording noise and flatten body oscillations due to limb movements, but short enough to warrant that, for this time step (i) the changes of heading/posture can be faithfully represented by orthodromic arcs, (ii) roll remains moderate ($|\rho_i| < \pi$) and (iii) linear, reorientation and rolling speeds remains approximately constant (but are allowed to markedly differ between time steps).

6. Relating rotations to changes of heading and posture

In 2D space, the posture is irrelevant and the heading is only defined by the azimuth, so that there is a single possible type of rotation, usually referred to as the turning angle, done in the animal's coronal plane. It therefore corresponds to yaw and is simply equal to the change of heading/azimuth. In 3D space, the change of heading is done in a plane that may be quite different from the animal's coronal plane, and therefore may involve both yaw and pitch. Furthermore, even if some roll does not change the heading, it involves a change in the orientation of the coronal plane with respect to the horizontal plane, and therefore affects how the change of heading can be decomposed in terms of yaw and pitch (Fig. 3). These terms are often misleadingly used to refer to the changes of azimuth, elevation angle and bank angle. The equivalence holds true only in three particular cases that are worth mentioning: (1) yaw

corresponds to a change of azimuth ($\alpha_i = \omega_i = \theta_i - \theta_{i-1}$) for a turn by α_i around the heave axis fixed vertically ($\phi_{i-1} = \phi_i = \lambda_{i-1} = \lambda_i = \beta_i = \rho_i = 0$); (2) pitch corresponds to a change of elevation angle ($\beta_i = \omega_i = \phi_i - \phi_{i-1}$ for a turn by β_i around the sway axis fixed horizontally without going beyond the vertical ($\lambda_{i-1} = \lambda_i = 0$, $\theta_i = \theta_{i-1}$, $\alpha_i = \rho_i = 0$); (3) roll corresponds to a change of bank angle ($\rho_i = \lambda_i - \lambda_{i-1}$) for a turn by ρ_i around the surge axis set to a fixed heading ($\theta_i = \theta_{i-1}$, $\phi_i = \phi_{i-1}$, $\alpha_i = \beta_i = \omega_i = 0$). In the general case involving any starting heading/posture, yaw, pitch and roll are related to changes of heading/posture in a much more complex way.

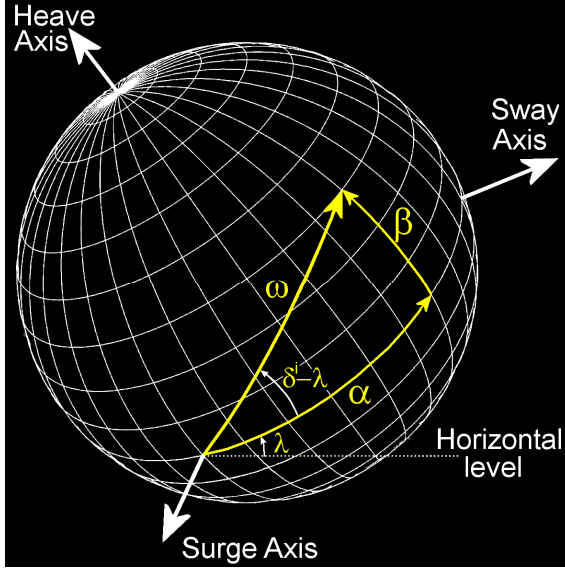


Fig. 3. Decomposition of the change of heading in terms of yaw and pitch. This reorientation can be suitably represented as an orthodromic arc drawn on a unit sphere in a pure body-bound frame of reference: the sphere is centered on the animal location, and the three reference axes correspond to the animal's main body axes. The rotation around the heave axis, i.e. yaw (α), and the rotation around the sway axis, i.e. pitch (β), done sequentially in this order, correspond to the two orthogonal components of the orthodromic arc representing the change of heading. They are related to the size (ω) and initial inclination (δ^i) of this arc, and to the bank angle (λ), by the expression $[\alpha_i \beta_i]^T = \mathbf{R}_1(\delta^i - \lambda)[\omega_i \mathbf{0}]^T$. In this sequential approach, roll is assumed to occur only before yaw and after pitch (its effect is already included in the λ value) so that the arc inclination expressed with respect to the animal's coronal plane remains constant (equal to $\delta^i - \lambda$) during the change of heading. Other formulae apply

when yaw, pitch and roll are done simultaneously (see text and Fig.4). In this example, the values of the different angles $\alpha = \pi/3$, $\beta = \pi/6$, $\omega \approx \pi/2.80$, $\delta^i - \lambda \approx \pi/5.34$ (replace π by 180 to obtain values in degrees). Note that δ^i and λ are 'surface' angles measured in the animal's frontal plane, i.e. the plane orthogonal to the surge axis, while α , β and ω are 'internal' angles whose vertex correspond to the center of the unit sphere.

If these three rotations are assumed to be done sequentially, with pitch done just after yaw (roll being done only before yaw / after pitch), yaw, α_i , and pitch, β_i , can be considered the two orthogonal components of heading at time t_i expressed in the frame of reference defined by the heading/posture at time t_{i-1} : $[\alpha_i \beta_i]^T = \mathbf{R}_1(-\lambda_{i-1})\mathbf{R}_2(-\phi_{i-1})\mathbf{R}_3(-\theta_{i-1})[\theta_i \phi_i]^T$. They can also be considered the two orthogonal components of the orthodromic arc that represents the change of heading between times t_{i-1} and t_i : $[\alpha_i \beta_i]^T = \mathbf{R}_1(\eta_i)[\omega_i \mathbf{0}]^T$, i.e.

$$\alpha_i = \text{atan2}(\cos(\eta_i), \cot(\omega_i)) \quad (12a)$$

$$\beta_i = \sin^{-1}(\sin(\eta_i) \sin(\omega_i)), \quad (12b)$$

where $\eta_i = \delta_i^i - \lambda_{i-1} = \delta_i^i - \lambda_i$ is the value, kept constant (no concomitant roll), of the reorientation inclination with respect to the animal's coronal plane (Fig. 3). It determines how the change of heading is shared between yaw and pitch, from pure yaw ($\eta_i = 0$ or $|\eta_i| = \pi$) to pure pitch ($|\eta_i| = \pi/2$). This sequential decomposition of the change of heading proves useful to model 3D RW in terms of yaw and pitch (Benhamou 2018). It suitably applies to small changes of heading/posture, as those involved when dealing with high-frequency estimates of

heading and posture, but will generate biased results if applied to heading/posture estimated at a lower frequency (every Δt). For example, when ω_i is large, they cannot account for the perfect balance between yaw and pitch ($|\alpha_i| = |\beta_i|$) that is expected when they are done simultaneously while the reorientation plane is at mid-way between the animal's coronal and sagittal planes (i.e. $|\eta_i| = \pi/4$ or $|\eta_i| = 3\pi/4$).

The simultaneous occurrence of rotational and translational movement components can be mimicked by virtually subdividing the change of heading/posture, from $(\theta_{i-1}, \phi_{i-1}, \lambda_{i-1})$ to $(\theta_i, \phi_i, \lambda_i)$, with roll $\rho_i = \eta_i^i - \eta_i^f$, in k sub-steps. The change of heading/posture performed for a given time step $\Delta t = t_i - t_{i-1}$ can then be modeled in a pseudo-continuous way as a series of k blocks of three successive elementary rotations, done in this order: (1) a rotation around the surge axis by ρ_i/k ; (2) a rotation around the heave axis by $\alpha_{i,j}$ and (3) a rotation around the sway axis by $\beta_{i,j}$, for $j = 1 \dots k$. Note that, to account for the concomitant change in location from \mathbf{x}_{i-1} to \mathbf{x}_i , the rotation around the surge axis has to be coupled with a translation along this axis by $\|\mathbf{x}_i - \mathbf{x}_{i-1}\| \sin(0.5\omega_i/k) / \sin(\omega_i/2)$, which corresponds to the length of the chord of an arc of circle with length $0.5\|\mathbf{x}_i - \mathbf{x}_{i-1}\|(\omega_i/k) / \sin(\omega_i/2)$ and radius $0.5\|\mathbf{x}_i - \mathbf{x}_{i-1}\| / \sin(\omega_i/2)$. The k sub-arcs modeling the change of heading have the same size, ω_i/k . Without roll, they are all characterized by the same yaw and pitch decomposition, i.e. $\alpha_{i,j} = \alpha_i/k$ and $\beta_{i,j} = \beta_i/k$ for any j . Otherwise, the incremental change by $-\rho_i/k$ of the reorientation inclination with respect to the animal's coronal plane, from η_i^i to η_i^f , leads each sub-arc to be decomposed in its own way: $\alpha_{i,j} = \tan^{-1}(\cos(\tilde{\eta}_i(q)) \tan(\omega_i/k))$ and $\beta_{i,j} = \sin^{-1}(\sin(\tilde{\eta}_i(q)) \sin(\omega_i/k))$, with $\tilde{\eta}_i(q) = \eta_i^i - q\rho_i$ and $q = j/k$. When k is sufficiently large to reliably model a continuous movement, these expressions can be rewritten $\alpha_{i,j} \approx \cos(\tilde{\eta}_i(q)) \omega_i/k$ and $\beta_{i,j} \approx \sin(\tilde{\eta}_i(q)) \omega_i/k$ (small-angle approximation). Yaw and pitch for the whole arc can therefore be expressed as $\alpha_i = \sum_j \alpha_{i,j} = \overline{\cos[\tilde{\eta}_i(q)]} \omega_i$ and $\beta_i = \sum_j \beta_{i,j} = \overline{\sin[\tilde{\eta}_i(q)]} \omega_i$. If roll is null, i.e. $\tilde{\eta}_i(q) = \eta_i$ for any q , one gets $\alpha_i = \cos(\eta_i)\omega_i$ and $\beta_i = \sin(\eta_i)\omega_i$, and therefore $|\alpha_i| = |\beta_i|$ for $|\eta_i| = \pi/4$ or $|\eta_i| = 3\pi/4$ as expected. Otherwise, with roll speed $\dot{\rho}_i = (\eta_i^i - \eta_i^f)/\Delta t$ considered constant for the short time step Δt , $\tilde{\eta}_i(q)$ is uniformly distributed between $\tilde{\eta}_i(0) = \eta_i^i = \bar{\eta}_i + \rho_i/2$ and $\tilde{\eta}_i(1) = \eta_i^f = \bar{\eta}_i - \rho_i/2$, where $\bar{\eta}_i = (\eta_i^i + \eta_i^f)/2$ is the mean value. Yaw and pitch for the time step $\Delta t = t_i - t_{i-1}$ can therefore be inferred as:

$$\alpha_i = (\sin(\eta_i^i) - \sin(\eta_i^f)) \omega_i / \rho_i = 2 \cos(\bar{\eta}_i) \sin(\rho_i/2) \omega_i / \rho_i \quad (13a)$$

$$\beta_i = (\cos(\eta_i^f) - \cos(\eta_i^i)) \omega_i / \rho_i = 2 \sin(\bar{\eta}_i) \sin(\rho_i/2) \omega_i / \rho_i, \quad (13b)$$

based on the values of ω_i , η_i^i and η_i^f derived from the heading/postures $(\theta_{i-1}, \phi_{i-1}, \lambda_{i-1})$ and $(\theta_i, \phi_i, \lambda_i)$, estimated from the accelero-magnetic measures made between times $t_{i-1} - \Delta t/2$ and $t_{i-1} + \Delta t/2$ and between times $t_i - \Delta t/2$ and $t_i + \Delta t/2$, respectively (Fig. 4).

Reciprocally, the 3D reorientation for the time step $\Delta t = t_i - t_{i-1}$ can be assessed from the actual values of yaw, pitch, and roll derived from angular speeds measured by a high-frequency tri-axial gyrometer (see §4). With a time step Δt sufficiently short to warrant that the angles obtained in this way remain in the range $[-\pi, \pi]$, the size of the change of heading and its mean inclination with respect to the animal's coronal plane can be computed as:

$$\omega_i = 0.5\rho_i(\alpha_i^2 + \beta_i^2)^{0.5}/\sin(\rho_i/2) \quad (14a)$$

$$\bar{\eta}_i = \text{atan2}(\beta_i, \alpha_i) \quad (14b)$$

By coupling postures $(\phi_{i-1}, \lambda_{i-1})$ and (ϕ_i, λ_i) estimated from the acceleration data recorded between times $t_{i-1}-\Delta t/2$ and $t_{i-1}+\Delta t/2$, and between times $t_i-\Delta t/2$ and $t_i+\Delta t/2$, respectively, and rotations α_i, β_i , and ρ_i estimated from gyrometric data recorded between times t_{i-1} and t_i , the change of azimuth between times t_{i-1} and t_i , $\Delta\theta_i = \theta_i - \theta_{i-1}$, can therefore be computed as

$$\Delta\theta_i = \text{atan2}(\sin(\omega_i)(\cos(\phi_{i-1})\cos(\delta_i^i) + \cos(\phi_i)\cos(\delta_i^f))/2, \cos(\omega_i) - \sin(\phi_{i-1})\sin(\phi_i)) \quad (15)$$

with $\delta_i^i = \lambda_{i-1} + \bar{\eta}_i + \rho_i/2$ and $\delta_i^f = \lambda_i + \bar{\eta}_i - \rho_i/2$.

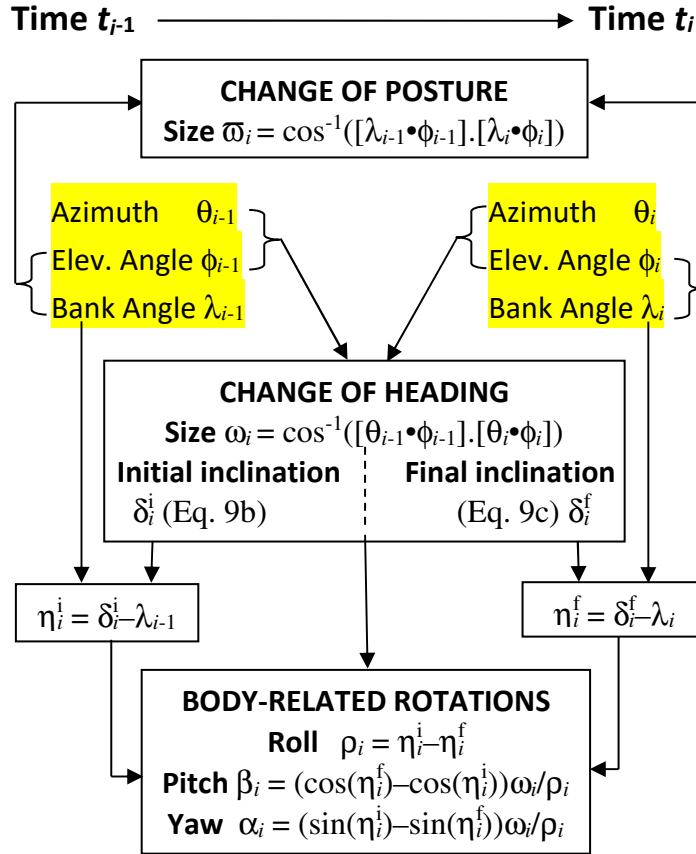


Fig. 4. Inferring body-related rotations from time series of heading/posture. An animal changes its heading (azimuth and elevation angle) and its posture (elevation and bank angles) through rotations – roll, pitch and yaw – done around its main three body axes – surge, sway and heave, respectively. These rotations can be inferred from the time series of successive headings and postures (expressed in the Earth-bound frame of reference specified by a geographical direction and gravity). The initial and final inclinations of reorientation expressed with respect to the body coronal plane (η_i^i and η_i^f) provides the interface between the body-bound and Earth-bound frames of reference that is required to convert changes of orientations into rotations. Recall: $[\xi \bullet \psi]$ stands for $(\cos(\xi) \cos(\psi), \sin(\xi) \cos(\psi), \sin(\psi))$.

7. KDE-based computation of spherical distributions

A useful way to assess a distribution rests on kernel density estimation (KDE; Silverman 1986). KDE generates smoothed histograms that do not depend on the arbitrary choice of the grid origin and bin size, which may bias the representation obtained with classical histograms. Furthermore, building a histogram on a sphere involves a tricky tessellation (Wilson et al.

2016). To apply KDE to locations on the plane, a virtual horizontal grid is overlaid on the environment and the density is estimated at the center of each cell of the grid by setting an isotropic bivariate kernel, usually Gaussian, on each location. The same principle applies to the locations on a unit sphere such as the ending points of 3D unit vectors $\boldsymbol{\mu}_i = [\xi_i, \psi_i]$ with $\xi_i \in [-\pi, \pi]$ (longitude-like) and $\psi_i \in [-\pi/2, \pi/2]$ (latitude-like). For this purpose, the horizontal planar grid is replaced by a spherical grid defined in terms of longitude-like and latitude-like value, and the isotropic bivariate Gaussian kernels are replaced by bivariate von Mises-Fisher kernels. In this way, KDE can apply to heading, (θ, ϕ) , change of heading, (δ^i, ω) , and posture, either (ϕ, λ) or (ζ, χ) , as azimuth, θ , initial arc inclination, δ^i , bank angle, λ , and postural orientation, χ , behave as longitudes, elevation angle, ϕ , behaves as a latitude, and arc size, ω , and overall inclination, ζ , behave as co-latitudes (i.e. $\pi/2 - \omega$ and $\pi/2 - \zeta$ behave as latitudes). Note however that this makes sense to compute a distribution (whichever the method used) only when the data is generated by a stationary process. Otherwise, the distribution obtained will arbitrarily depend on when the data considered begins and ends to be collected. It is therefore advised to check whether the mean and the variance obtained for the first, second, and third thirds of the time series of the data considered remain similar (Benhamou 2014) before attempting to build the distribution.

For any location \mathbf{x} on the unit sphere, the $\boldsymbol{\mu}$ -centered bivariate von Mises-Fisher probability density function with concentration parameter κ is

$$f(\mathbf{x}) = \kappa \exp(\kappa \cos(\Omega_{\mathbf{x}, \boldsymbol{\mu}})) / (4\pi \sinh(\kappa)) \quad (16a)$$

where $\Omega_{\mathbf{x}, \boldsymbol{\mu}}$ is the size of the orthodromic arc $\widehat{\mathbf{x}\boldsymbol{\mu}}$. The mean vector length of this distribution is $E(\cos(\Omega_{\mathbf{x}, \boldsymbol{\mu}})) = \coth(\kappa) - 1/\kappa$ (Fisher 1953; see Ahmed et al. 2021 for additional details). Call $\|\mathbf{x} - \boldsymbol{\mu}\|$ the straight distance between the mean location $\boldsymbol{\mu}$ and any given location \mathbf{x} on the unit sphere, which therefore corresponds to the chord length of the arc $\widehat{\mathbf{x}\boldsymbol{\mu}}$. One gets $\cos(\Omega_{\mathbf{x}, \boldsymbol{\mu}}) = 1 - (\mathbf{x} - \boldsymbol{\mu})^2/2$. Furthermore, with $\kappa > 6$, one gets $\sinh(\kappa) \approx \cosh(\kappa) \approx \exp(\kappa)/2$. The von Mises-Fisher distribution with $\kappa > 6$ can therefore be suitably approximated as:

$$f(\mathbf{x}) \approx \exp(-0.5(\mathbf{x} - \boldsymbol{\mu})^2/\sigma^2) / (2\pi\sigma^2) \quad (16b)$$

with $\sigma^2 = 1/\kappa \approx 1 - E(\cos(\Omega_{\mathbf{x}, \boldsymbol{\mu}}))$. Thus, a $\boldsymbol{\mu}$ -centered bivariate von Mises-Fisher distribution with concentration parameter $\kappa > 6$ (i.e. $\sigma < \pi/2.45$) and a zero-centered isotropic bivariate Gaussian distribution with variance $\sigma^2 = 1/\kappa$ reflect each other through a $\boldsymbol{\mu}$ -centered Lambert azimuthal equal-area projection, which maps orthodromic arcs originating at $\boldsymbol{\mu}$ as their corresponding chords. Consequently, the area encompassed within a given cumulative isopleth is the same for both distributions.

The standard-deviation of a distribution used as a kernel in KDE is usually referred to as the smoothing parameter (or bandwidth) h . The value required to reliably estimate a spherical distribution is unlikely to be larger than $\pi/2.45$ (with $h = \pi/2.45$, the 0.95 cumulative isopleth of a von Mises-Fisher distribution is a circle that delimits a cap corresponding to 1/4 of the sphere area). Consequently, although approximate, Eq. (16b) should act as an appropriate

kernel for building most (if not all) KDE-based spherical distributions. The density at the center $\mathbf{c} = [\xi_c, \psi_c]$ of a given cell of the spherical grid can therefore be estimated as

$$U_c = \frac{1}{2\pi n h^2} \sum_{i=1}^n \exp\left(-\frac{(\mathbf{c} - \mathbf{\mu}_i)^2}{2h^2}\right) \quad (17)$$

This expression is identical to the Gaussian kernel-based expression that applies to planar distributions if one agrees that $(\mathbf{c} - \mathbf{\mu})^2$ is the squared Euclidean distance between \mathbf{c} and $\mathbf{\mu}$: $(\mathbf{c} - \mathbf{\mu})^2 = (x_c - x_\mu)^2 + (y_c - y_\mu)^2$ on the plane vs. $(\mathbf{c} - \mathbf{\mu})^2 = (x_c - x_\mu)^2 + (y_c - y_\mu)^2 + (z_c - z_\mu)^2$, with $x = \cos(\xi) \cos(\psi)$, $y = \sin(\xi) \cos(\psi)$, and $z = \sin(\psi)$, on the unit sphere, i.e.

$$(\mathbf{c} - \mathbf{\mu}_i)^2 = 2(1 - \sin(\psi_c) \sin(\psi_i) - \cos(\psi_c) \cos(\psi_i) \cos(\xi_i - \xi_c)) \quad (18)$$

When KDE applies to locations on a plane $\mathbf{x}_i = (x_i, y_i)$ that are independent of each other and come from an isotropic bivariate Gaussian distribution with standard deviation σ , the best trade-off between a level of smoothing sufficiently high to eliminate noise and sufficiently low to keep relevant information is given by $h_{\text{ref}} = \sigma/n^{1/6}$ (Silverman 1986). When dealing with 3D orientations $\mathbf{\mu}_i = [\xi_i, \psi_i]$, the corresponding value is $h_{\text{ref}} = \kappa^{0.5}/n^{1/6} = (1 - \|\sum_i [\xi_i, \psi_i]\|/n)^{0.5}/n^{1/6}$ (see example in Fig. 5). However, as this double assumption never holds true, the h_{ref} value only provides an order of magnitude of the value of smoothing parameter required for reliably representing the distribution.

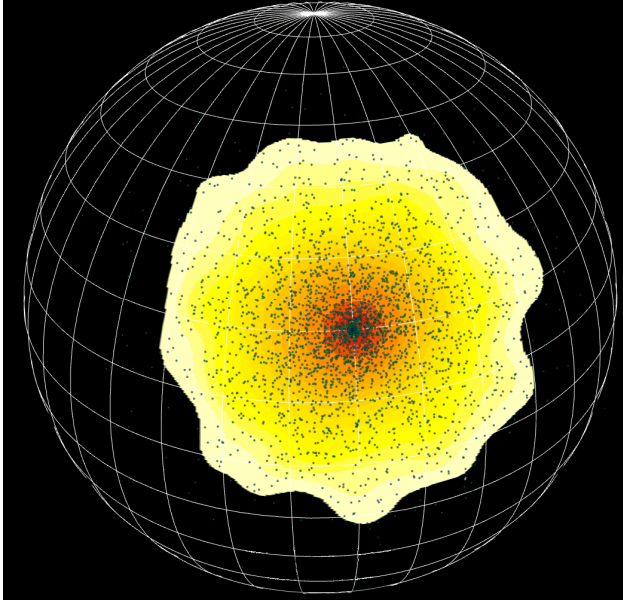


Fig. 5. KDE-based distribution of 3D orientations (i.e. locations on a unit sphere). In this example based on computer simulations, $n = 3000$ locations (dark green dots) were drawn independently of each other from a bivariate von Mises-Fisher distribution centered on location $[0, \pi/6]$ with concentration parameter $\kappa = 31.5$ (corresponding to standard-deviation $\sigma = \pi/18$). The KDE was obtained using von Mises-Fisher kernels centered on each location with a smoothing parameter $h = \kappa^{0.5}/n^{1/6} \approx \pi/68$. The density level decreases from the red area to the pale yellow area. The overall area has been cut at the 0.95 cumulative isopleth. In this particular example, any cumulative isopleth is theoretically a circle, but the low density in the peripheral areas makes them highly sensitive to random sampling fluctuations.

The fraction of distribution attributed to a given \mathbf{c} -centered cell of the virtual spherical grid is equal to $a_c U_c$, where a_c is the cell area. If the grid is based on a regular binning of longitudes-like ξ and latitudes-like ψ with angular bin size υ , the cell area is variable: $a_c = 2\upsilon \sin(\upsilon/2) \cos(\psi_c) \approx \upsilon^2 \cos(\psi_c)$. A grid with a constant cell area $a_c = \upsilon s$ can be defined through a regular binning of longitudes-like and sines of latitudes-like, with bin sizes υ and s , respectively. To compute the smallest area encompassed within a given cumulative isopleth (such as the 0.95 and 0.50 ones classically used to determine the overall distribution and its

core areas), the cells of the virtual grid involved in the computation have to be sorted in the decreasing order of the densities and the corresponding fractions has to be summed up until the cumulative isopleth value is reached. The portion of area one looks for then corresponds to the set of the cells involved by this summation. When cells have all the same area, fractions and densities are proportional to each other. Sorting and summing can then be both performed using a single variable (density or fraction). When the cell area is variable, the procedure is just a bit more complex: sorting densities and summing the corresponding fractions must be made jointly in parallel rather than as a single operation.

Thus, KDE applies to planar and spherical distributions quite similarly. This holds true for both the location-based (i.e. classical) version (LKDE) and the movement-based version (MKDE). MKDE is more suitable than LKDE when the locations are highly serially correlated, as occurred when dealing with 3D orientation. It extends LKDE by setting kernels (with a variable smoothing parameter) on in-between interpolated locations to simulate random bridges linking successive recorded locations (Benhamou 2011). With this approach the overall distribution can not only be assessed, but also decomposed in terms of spatial distributions of the frequency of visits and of the mean time spent per visit (Benhamou & Riotte-Lambert 2012). A program designed to compute these different distributions for 3D orientations, BRB/MKDE_ORI3D (including LKDE as a particular case), can be freely downloaded from www.cefe.cnrs.fr/fr/recherche/bc/dpb/216-simon-benhamou.

8. Fine-scale movement reconstruction

The data acquired by high-frequency tri-axial accelero-magnetometers, and possibly a speedometer, makes it possible to infer fine-scale movements between successive relocations of animals that cannot be tracked with a very high frequency. This is in particular the case of aquatic animals such as marine mammals, sea turtles, or penguins, which can be GNSS-relocated only when they come to the surface to breath. For non-aquatic animals tracked over long periods, a relatively low relocation frequency may also have been deliberately chosen to spare the battery of the on-board GNSS receptor. Fine-scale movement reconstruction is often referred to as dead-reckoning, because it is somewhat similar to the way ancient navigators kept track at sea of the compass-bearing of the harbor.

The successive animal's locations are computed recurrently as $\mathbf{x}_i = (x_i, y_i, z_i) = \mathbf{x}_{i-1} + \mathbf{v}_i \Delta t$, where \mathbf{v}_i is the animal's velocity for the i^{th} time step. The norm of this vector corresponds to the speed, v_i , and its orientation corresponds to the heading (θ_i, ϕ_i) . Such a recurrent procedure is however prone to accumulate random errors due to the various noises affecting the speed, magnetic and acceleration measures, from which \mathbf{v}_i is derived. It can therefore work reliably only for relatively short delays between ground-truth, GNSS-based relocations used as 'anchors' to compel the reconstructed movement bouts to start and end at these relocations.

The principle for estimating the heading from tri-axial accelero-magnetic data is detailed in §3. Note however that, here, heading (θ_i, ϕ_i) applies to the step $\mathbf{x}_{i-1} \rightarrow \mathbf{x}_i$ rather than to the t_i time-stamped location \mathbf{x}_i . It should therefore be assessed from the accelero-magnetic data recorded between times t_{i-1} and t_i rather than between $t_i - \Delta t/2$ and $t_i + \Delta t/2$. The forward speed v_i can theoretically be estimated by time-integrating the surge acceleration signal, but this signal is usually far too noisy for this purpose. Despite swimming animals move in a smoother way than terrestrial ones, other methods had to be developed to estimate their speed, e.g. a bending paddle (Wilson et al. 2008), a passive propeller (Shiomi et al. 2008) or recording the sound level of the water flow against the body (Le Bras et al. 2017). For terrestrial animals, a possibility would be to use the visual flow from the ground, but the amount of energy it requires would prevent this technique from being usable continuously for extended periods. Fortunately, as the reconstructed movement will be stretched or shrunk to start and end at GNSS-based 'anchors' (see below), one only needs a proxy \tilde{v}_i that is proportional to the actual speed v_i . Without a device that can act as a speedometer, DBA can be considered a speed proxy, with some limitations. Indeed, for numerous species, DBA appears to be roughly proportional to the speed (Bidder et al. 2012). However, passive gliding in air or water is characterized by the same very low DBA as resting, while a high DBA value can be associated with a null speed when the animal is shaking its body on the spot. A detailed analysis of the acceleration and magnetic signals might help highlight these active phases involving a null speed.

Movement reconstruction involves merging the velocity data with ground-truth (GNSS-based) relocations used as 'anchors' to specify the start and end of each reconstructed movement bout. This procedure removes the systematic errors that may affect the azimuth (e.g. due to neglecting the magnetic declination) and the speed (due to considering only a speed proxy proportional to the actual speed). The accelero-magnetometer (and speedometer, if any) measures are usually time-stamped with an independent clock. If so, these measures must be synchronized with GNSS relocations manually, to the closest second, e.g. by inducing a short and strong acceleration at a precise GNSS time, at the beginning of the tracking period, and if possible (battery still alive), at its end, so as to correct for a possible a time drift of the accelero-magnetometer clock. For marine animals breathing at the surface and equipped with a time-depth recorder (TDR) sharing the same clock as the accelero-magnetometer, the synchronization with GNSS locations can also be done based on surfacing events, as no relocation can be recorded when the animal is underwater. I will first detail the general approach that applies to 3D movements. The simplified version that applies to 2D movements of terrestrial animals for which the logger is set in a collar rather than tightly set on the back will presented afterwards.

Consider the overall movement defined by a series of N GNSS-based relocations, expressed in terms of longitudes (Ξ_l), latitudes (Ψ_l), and altitudes or depths (Z_l), recorded at

times T_I , for $I = 0 \dots N-1$. For animals that move over limited extents, longitudes and latitudes can be converted into Cartesian coordinates, (X_I, Y_I) , through a small-extent metric projection (e.g. UTM). Otherwise, the arc-step linking any two successive relocations (Ξ_{I-1}, Ψ_{I-1}) and (Ξ_I, Ψ_I) is usually sufficiently short to be suitably converted into a vector-step through a simple local flat-Earth approximation. In this case, a convenient solution for reconstructing the movement bout between times T_{I-1} and T_I consists in (i) setting $X_{I-1} = 0$, $Y_{I-1} = 0$, $X_I = R(\Xi_I - \Xi_{I-1})\cos((\Psi_{I-1} + \Psi_I)/2)$ and $Y_I = R(\Psi_I - \Psi_{I-1})$, where $R = 6,371,000$ m is the mean Earth radius and longitudes and latitudes are expressed in radians, (ii) computing the dead-reckoned Cartesian coordinates x_i and y_i of in-between locations (see below), and (iii) back-converting x_i into longitude, $\xi_i = \Xi_{I-1} + x_i/(R\cos((\Psi_{I-1} + \Psi_I)/2))$, and y_i in latitude, $\psi_i = \Psi_{I-1} + y_i/R$.

In any case, the I^{th} step $(\Delta X_I, \Delta Y_I, \Delta Z_I)$, with $\Delta X_I = X_I - X_{I-1}$, $\Delta Y_I = Y_I - Y_{I-1}$, and $\Delta Z_I = Z_I - Z_{I-1}$, can be represented by the ground-truth vector $L_I[\Theta_I \bullet \Phi_I]$, with length $L_I = ((\Delta X_I)^2 + (\Delta Y_I)^2 + (\Delta Z_I)^2)^{0.5}$, azimuth $\Theta_I = \text{atan2}(\Delta Y_I, \Delta X_I)$ and elevation angle $\Phi_I = \sin^{-1}(\Delta Z_I/L_I)$. This step can also be assessed as the dead-reckoned vector $\tilde{V}_I \Delta t [\hat{\Theta}_I \bullet \hat{\Phi}_I] = \sum_i \tilde{v}_i \Delta t [\theta_i \bullet \phi_i]$, for $i = 1 \dots n = \text{round}((T_B - T_A)/\Delta t)$, where \tilde{v}_i , θ_i and ϕ_i are the speed proxy, body azimuth and body elevation angle estimated for each elementary time step Δt . The overall speed proxy, azimuth and elevation angle of the dead-reckoned vector are therefore $\tilde{V}_I = (\sum_i^2 \tilde{v}_{xi} + \sum_i^2 \tilde{v}_{yi} + \sum_i^2 \tilde{v}_{zi})^{0.5}$, $\hat{\Theta}_I = \text{atan2}(\sum_i \tilde{v}_{yi}, \sum_i \tilde{v}_{xi})$ and $\hat{\Phi}_I = \sin^{-1}(\sum_i \tilde{v}_{zi}/\tilde{V}_I)$, with $\tilde{v}_{xi} = \tilde{v}_i \cos(\phi_i) \cos(\theta_i)$, $\tilde{v}_{yi} = \tilde{v}_i \cos(\phi_i) \sin(\theta_i)$ and $\tilde{v}_{zi} = \tilde{v}_i \sin(\phi_i)$. Systematic errors and the accumulation of random errors result in a dead-reckoned vector that does not match the ground-truth vector. As all these errors come from misestimates in terms of orientation and length, the dead-reckoned movement must be corrected in polar (rather than Cartesian) terms, through rotation and rescaling (i.e. stretching or shrinking), to preserve its overall shape.

The orientation error can be corrected by rotating the dead-reckoned vector first by $-\hat{\Theta}_I$ around the X axis (i.e. in the horizontal plane) to get its azimuth pointing eastwards, then by $\Phi_I - \hat{\Phi}_I$ around the Y axis (i.e. in the E-W vertical plane) to correct its elevation angle without changing its azimuth, and finally by Θ_I around the X axis (i.e. in the horizontal plane) to fully align it onto the ground truth vector. The error in length can be corrected by rescaling the dead-reckoned vector by $L_I/(\tilde{V}_I \Delta t)$. The orientation adjustment and rescaling apply similarly to every step. With \mathbf{x}_0 set to \mathbf{X}_{I-1} , the series of subsequent locations $\mathbf{x}_i = (x_i, y_i, z_i)$, for $i = 1 \dots n_I$, specifying the path performed between the two successive ground-truth relocations, can therefore be computed recurrently as $\mathbf{x}_i^T = \mathbf{x}_{i-1}^T + \mathbf{R}_3(\Theta_I) \mathbf{R}_2(\Phi_I - \hat{\Phi}_I) \mathbf{R}_3(-\hat{\Theta}_I) \tilde{\mathbf{v}}_i^T L_I / \tilde{V}_I$, i.e.

$$x_i = x_{i-1} + (r_i \cos(\Theta_I) - q_i \sin(\Theta_I)) L_I / \tilde{V}_I \quad (19a)$$

$$y_i = y_{i-1} + (q_i \cos(\Theta_I) + r_i \sin(\Theta_I)) L_I / \tilde{V}_I \quad (19b)$$

$$z_i = z_{i-1} + (\tilde{v}_{zi} \cos(\Phi_I - \hat{\Phi}_I) + p_i \sin(\Phi_I - \hat{\Phi}_I)) L_I / \tilde{V}_I \quad (19c)$$

with $p_i = \tilde{v}_{xi} \cos(\hat{\Theta}_I) + \tilde{v}_{yi} \sin(\hat{\Theta}_I)$, $q_i = \tilde{v}_{yi} \cos(\hat{\Theta}_I) - \tilde{v}_{xi} \sin(\hat{\Theta}_I)$ and $r_i = p_i \cos(\Phi_I - \hat{\Phi}_I) - \tilde{v}_{zi} \sin(\Phi_I - \hat{\Phi}_I)$. This formulation warrants that the dead-reckoned movement between times T_{I-1} and T_I starts at \mathbf{X}_{I-1} and ends at \mathbf{X}_I . The location errors at intermediate times tend to increase

with the delay $T_I - T_{I-1}$, which should therefore be kept as small as possible, in particular when the speed is poorly estimated.

For marine animals that breathe at the sea surface ($Z_{I-1} = Z_I = 0$), Eqs (19) apply with $\Phi_I = 0$ and $L_I = ((\Delta X_I)^2 + (\Delta Y_I)^2)^{0.5}$. Furthermore, the dead-reckoned z_i values should be replaced by TDR-based ones, if available, as they are more accurate. It is also worth noting that the speed proxy of marine animals applies to the swimming, i.e. water masses-related movement, whereas the GNSS-based relocations used as 'anchors' are expressed in a ground-bound frame of reference. When the water speed is not negligible with respect to the animal's swimming speed, the ground-related vectors linking successive GNSS relocations should first be translated into water-related ones (through vector subtraction; see details in Girard et al. 2006). The swimming movement bouts between two successive water masses-related GNSS relocations are then reconstructed following the standard procedure. Finally, if the geographical information matters (e.g. for relating the animal's location with some habitat characteristics), the fine-scale swimming movement may be converted (through vector addition) into a fine-scale ground-related movement.

For a collared terrestrial animal, the device's posture can dramatically differ from the body posture, and vary during movement because the collar is liable to roll around the neck. At least, the azimuth of the device can be computed as (similar to Eq. 6)

$$\theta^d = \text{atan2}((\bar{a}_v^2 + \bar{a}_w^2) \bar{m}_u - \bar{a}_u(\bar{a}_v \bar{m}_v + \bar{a}_w \bar{m}_w), (\bar{a}_v \bar{m}_w - \bar{a}_w \bar{m}_v) \|\bar{\mathbf{a}}\|). \quad (20)$$

Provided the surge axis of the device lies in the sagittal plane, the body azimuth can be computed as $\theta = \theta^d - \text{atan2}(q, p)$ with $(p, q, r)^T = \mathbf{R}_2(\phi)\mathbf{R}_1(\lambda)[0 \bullet \phi^*]^T$, i.e.

$$\theta = \theta^d + \text{atan2}(\sin(\phi^*) \sin(\lambda), \cos(\phi^*) \cos(\phi) - \sin(\phi^*) \sin(\phi) \cos(\lambda)) \quad (21)$$

where ϕ^* is the angular discrepancy between the surge axes of the device and the body. Eq. (21) results in the exact same θ value as Eq. (6). The device must be set on the collar so that its surge axis is orthogonal to the collar plane. This warrants that this axis remains in the body sagittal plane whatever the collar orientation. However, contrarily to what happens with a device tightly set on the animal's back, ϕ^* varies unpredictably with a device set on a collar. This does not prevent Eq. (21) from being applied to terrestrial animals because, fortunately, such animals can be expected to always move unbanked ($\lambda = 0$), leading to $\theta = \theta^d$ whatever the value of ϕ^* . Furthermore, as the movements of terrestrial animals are mostly restricted to the horizontal plane ($\Phi_I = \hat{\Phi}_I = 0$; $\tilde{v}_{zi} = 0$ for any i), the z coordinates are irrelevant and the x and y coordinates are obtained recurrently simply as:

$$x_i = x_{i-1} + (\cos(\Theta_I - \hat{\Theta}_I) \tilde{v}_{xi} - \sin(\Theta_I - \hat{\Theta}_I) \tilde{v}_{yi}) L_I / \tilde{V}_I \quad (22a)$$

$$y_i = y_{i-1} + (\cos(\Theta_I - \hat{\Theta}_I) \tilde{v}_{yi} + \sin(\Theta_I - \hat{\Theta}_I) \tilde{v}_{xi}) L_I / \tilde{V}_I \quad (22b)$$

$$= y_{i-1} + ((\Delta X_I \Sigma_i \tilde{v}_{xi} + \Delta Y_I \Sigma_i \tilde{v}_{yi}) \tilde{v}_{xi} - (\Delta Y_I \Sigma_i \tilde{v}_{xi} - \Delta X_I \Sigma_i \tilde{v}_{yi}) \tilde{v}_{yi}) / (\Sigma_i^2 \tilde{v}_{xi} + \Sigma_i^2 \tilde{v}_{yi}).$$

with $\tilde{v}_{xi} = \tilde{v}_i \cos(\theta_i)$ and $\tilde{v}_{yi} = \tilde{v}_i \sin(\theta_i)$. An example is shown in Fig. 6. When estimated at a relatively high frequency (e.g. with $\Delta t = 1$ s) the two speed components, \tilde{v}_{xi} and \tilde{v}_{yi} , tends to be

very noisy because the rough locomotion mode of terrestrial animals tends to strongly shake the device. Some smoothing (e.g. by simply by sub-sampling the inferred locations to keep a single location every few seconds or by applying a sliding window with a width of a few seconds) is therefore often necessary.

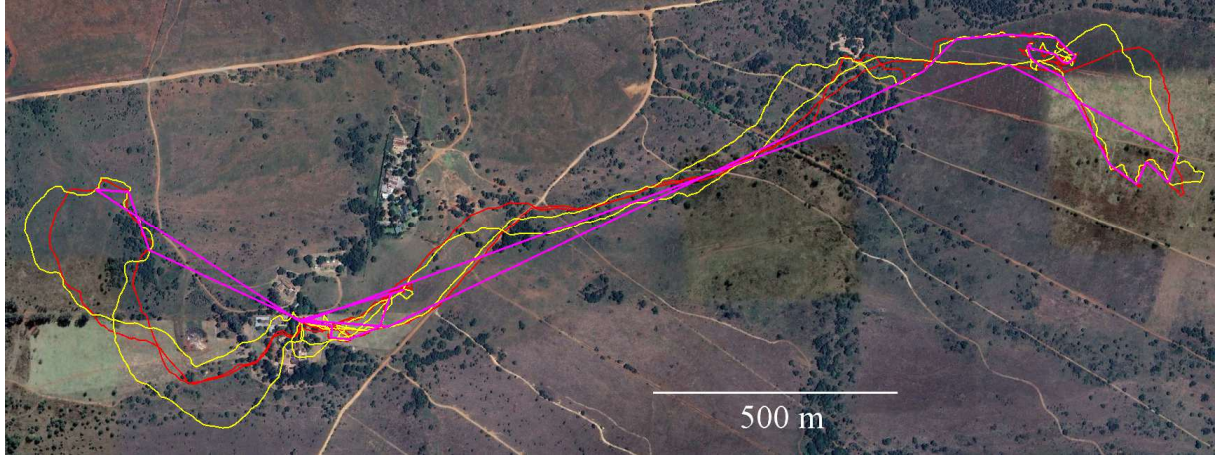


Fig. 6. Reconstructed path of a domestic free-ranging horse tracked for 24h (based on unpublished data recorded Jodie Martin). The horse was GPS-tracked with a relocation every 10 s, to obtain a faithful path representation (drawn in red). The GPS relocations were subsampled to one every 30 min. to obtain the kind of path representation that is usually obtained when tracking wild animals (drawn in magenta). Then, the data acquired by an on-board tri-axial high-frequency accelero-magnetometer were used to reconstruct the path between 30-min GPS relocations (drawn in yellow) using Eqs (22).

9. Conclusions

On-board tri-axial high-frequency accelerometers, magnetometers and gyroscopes, alone or coupled, have become cheaper and less energy-consuming. This makes it possible to record data on more individuals belonging to smaller species or for longer durations. The present was written with the aim to help the researchers who wish to address questions that require this type of data to compute the key variables and represent their distributions more easily.

Beyond the various trigonometric expressions that are required to compute heading/posture (and possibly relate their changes in terms of body-related rotations) from raw accelero-magnetic data, a recurrent issue with tri-axial high-frequency devices working continuously comes from the huge amount of raw data to manage. It is however worth noting that the successive raw data values acquired at high-frequency are both noisy and highly serially correlated. This means that amount of information they provide is much lower than the amount of data. The derived variables such as heading and posture can be estimated at the same high frequency f as the one used to acquire the raw data using a Δt -width *sliding* window which can dramatically smooths the signal (i.e. remove a lot of noise). However, this procedure also dramatically increases the level of serial correlation mechanically (with a sliding window encompassing $k = \text{round}(f\Delta t)$ values, the range of values considered a given time and at the next time shared $k-1$ values), so that the information provided by the change of heading and posture for the very short time $1/f$ is likely to be insignificant. Using a Δt -width

jumping rather than *sliding* window will smooth the signal as well. With this approach, the amount of data to store and to process in subsequent analyses is dramatically reduced (by $f\Delta t$, as a single value of heading/posture is kept for each time step Δt), and the level of serial correlation is reduced as well, so that most information present in the signal is preserved. If necessary, in-between values can be inferred through interpolation (Eqs 11) and the associated body-related rotations raw, pitch and roll for the time step Δt considered can be also be easily inferred (Fig. 8). For purely technical reasons, posture has to be initially computed at high-frequency using a *sliding* window to assess DBA, which is then also assessed at the same high frequency. However, only a single value of posture (through sub-sampling), and of DBA (through averaging) need to be kept for each time step Δt . Obviously, its width must be carefully chosen: it should be just long enough to suitably smooth fast acceleration fluctuations due to locomotion (see Shepard et al. 2008a), so as to keep the data resolution as high as possible. It is also worth noting that activity level can be reliably estimated using a low-frequency accelerometer (Benoit et al. 2020). A high-frequency tri-axial accelerometer is therefore really necessary if one is also interested by reliably assessing body posture.

It may be necessary to keep the whole time series of raw data for performing complex analyses such as spectral analyses to detect and characterize regular body oscillations (e.g. Williams et al. 2017). However, there often exist simpler and lighter alternatives. For instance, such oscillations in a flying bird, due to wing movements, can be detected and characterized more simply by keeping only two values for each time step Δt : the mean \bar{d} and the coefficient of variation, CV, of the delay between successive times at which the heave component of acceleration goes through a balance point equal to $-g$. Random fluctuations involves that the delay is exponentially distributed (CV=1). Regular oscillations can therefore be detected by $CV \ll 1$, and their period can then be estimated as $T = 2\bar{d}$ (for $\bar{d} > 1/f$; Nyquist criterion). Based on this approach and on the value of the elevation angle ϕ , kestrel falcons could be said to hover ($\phi \approx 0$, $CV < 0.5$, $T < 150$ ms), perform flapped ($\phi \approx 0$; $CV < 0.5$, $T \in [150, 220]$ ms) or glided ($\phi \approx 0$; $CV > 0.5$) fly, or to be perched ($\phi > 0$, $CV > 0.5$; García Silveira, unpublished results). For sea turtles, which swim using a forward-backward movement of front flippers, a similar analysis can be done by considering the surge component of acceleration with respect to a balance point equal to $\sin(\phi)g$.

As these examples show, some behaviors can be inferred by comparing values derived from the data acquired by bio-loggers to relevant thresholds (see also Shepard et al. 2008b). However, when quite different behaviors generate relatively similar signals, this simple approach does not work. Machine learning then can help to infer behavior from 'big data' acquired by on-board loggers (Jeantet et al. 2020, 2021). It should nevertheless be keep in mind that learning will be faster and/or more easily applicable if the machine is fed with biologically relevant parameters such as, for example, DBA and elevation and bank angles rather than on raw acceleration data. Correcting the parameters that apply to the device to

obtain those that apply to the body (Eqs 1, 5 and 7) should also avoid that the results obtained were blurred by the discrepancy between the two frames of references, which may vary between individuals. In other terms, an approach based on artificial intelligence will work all the better if it is supported by human intelligence.

References

- Ahmed D.A., Benhamou S., Bonsall M.B. & Petrovskii S.V. 2021. Three-dimensional random walk models of individual animal movement and their application to trap counts modelling. *J. Theor. Biol.* 524: 110728
- Benhamou S. 2011. Dynamic approach to space and habitat use based on biased random bridges. *PLoS ONE* 6, e14592.
- Benhamou S. 2014. Of scales and stationarity in animal movements. *Ecol. Let.* 17, 261–272.
- Benhamou S. 2018. Mean squared displacement and sinuosity of three-dimensional random search movements. *arXiv*:1801.02435
- Benhamou S. & Riotte-Lambert L. 2012. Beyond the utilization distribution: Identifying home range areas that are intensively exploited or repeatedly visited. *Ecol. Model.* 227: 112–116.
- Benoit L., Hewison, A.J., Coulon A., Debeffe L., Grémillet D., Ducros D., Cargnelutti B., Chaval Y. & Morellet N. 2020. Accelerating across the landscape: the energetic costs of natal dispersal in a large herbivore. *J. Anim. Ecol.* 89: 173–185.
- Bidder O.R., Soresina M., Shepard E.L., Halsey L.G., Quintana F., Gómez-Laich A. & Wilson R.P. 2012. The need for speed: testing acceleration for estimating animal travel rates in terrestrial dead-reckoning systems. *Zool.* 115: 58–64
- Fisher R.A 1953. Dispersion on a sphere. *Proc. R. Soc. Lond. A* 217: 295–305.
- Girard C., Sudre J., Benhamou S., Roos D. & Luschi P. 2006. Homing in green turtles (*Chelonia mydas*): oceanic currents act as a constraint rather than as an information source. *Marine Ecology Progress Series* 322, 281–289.
- Gleiss A.C., Wilson R.P. & Shepard E.L. 2011. Making overall dynamic body acceleration work: on the theory of acceleration as a proxy for energy expenditure. *Meth. Ecol. Evol.* 2: 23–33.
- Jeantet L., Planas-Bielsa V., Benhamou S., et al. 2020. Behavioural inference from signal processing using animal-borne multi-sensor loggers: a novel solution to extend the knowledge of sea turtle ecology. *R. Soc. Open Sci.* 7: 200139.
- Jeantet L., Vigon V., Geiger S. & Chevallier D. 2021. Fully convolutional neural network: A solution to infer animal behaviours from multi-sensor data. *Ecol. Model.* 450: 109555.
- Johnson M.P. & Tyack P.L 2003. A digital acoustic recording tag for measuring the response of wild marine mammals to sound. *IEEE J. Ocean. Engin.* 28: 3–12.

- Le Bras Y., Jouma'a J. & Guinet C. 2017. Three-dimensional space use during the bottom phase of southern elephant seal dives. *Mov. Ecol.* 5: 18.
- Qasem L., Cardew A., Wilson A., et al. 2012. Tri-Axial dynamic acceleration as a proxy for animal energy expenditure; should we be summing values or calculating the vector? *PLoS ONE* 7: e31187.
- Shepard E.L., Wilson R.P., Halsey L.G., et al. 2008a. Derivation of body motion via appropriate smoothing of acceleration data. *Aquat. Biol.* 4: 235–241.
- Shepard E.L., Wilson R.P., Quintana F., et al. 2008b. Identification of animal movement patterns using tri-axial accelerometry. *Endang. Species Res.* 10: 47–60.
- Shiomi K., Sato K., Mitamura H., Arai N., Naito Y. & Ponganis P.J. 2008. Effect of ocean current on the dead-reckoning estimation of 3-D dive paths of emperor penguins. *Aquat. Biol.* 3: 265–270.
- Silverman B.W. 1986. *Density estimation for statistics and data analysis*. Boca Raton, Florida, USA: Chapman & Hall/CRC. 175 p.
- Williams H.J., Shepard E.L., Duriez O. & Lambertucci S.A. 2015. Can accelerometry be used to distinguish between flight types in soaring birds? *Anim. Biotelem.* 3: 45.
- Williams H.J., Holton M.D., Shepard E.L., et al. 2017. Identification of animal movement patterns using tri-axial magnetometry. *Mov. Ecol.* 5: 6.
- Williams H.J., Taylor L.A., Benhamou S., et al. 2020. Optimising the use of bio-loggers for movement ecology research. *J. Anim. Ecol.* 89: 186–206.
- Wilson A.M., Lowe J.C., Roskilly K., Hudson P.E., Golabek K.A. & McNutt J.W. 2013. Locomotion dynamics of hunting in wild cheetahs. *Nature* 498: 185–189.
- Wilson R.P., White C.R., Quintana F., Halsey L.G., Liebsch N., Martin G.R. & Butler P.J. 2006. Moving towards acceleration for estimates of activity-specific metabolic rate in free-living animals: the case of the cormorant. *J. Anim. Ecol.* 75: 1081–1090.
- Wilson R.P., Holton M.D., Walker J.S., et al. 2016. A spherical-plot solution to linking acceleration metrics with animal performance, state, behaviour and lifestyle. *Mov. Ecol.* 4: 22.
- Wilson R.P., Börger L., Holton M.D., et al. 2020. Estimates for energy expenditure in free-living animals using acceleration proxies: A reappraisal. *J. Anim. Ecol.* 89:161–172.